Galactic coronae in the intracluster environment: semiconfined stellar-feedback-driven outflows

Mon. Not. R. Astron. Soc. **000**, 000–000 (0000) Printed 4 January 2011 (MN LATEX style file v2.2)

Galactic Coronae in the Intracluster Environment: Semi-confined Stellar-feedback-driven Outflows

Zhankui Lu[1] ⋆ and Q. Daniel Wang[1]
[1] *Department of Astronomy at University of Massachusetts, Amherst, 01003, USA*

ABSTRACT
Recently X-ray observations have shown the common presence of compact galactic coronae around intermediate-mass spheroid galaxies embedded in the intracluster/intragroup medium (ICM). We conduct 2-D hydrodynamic simulations to study the quasi-steady-state properties of such coronae as the natural products of the ongoing distributed stellar feedback semi-confined by the thermal and ram pressures of the ICM. We find that the temperature of a simulated corona depends primarily on the specific energy of the feedback, consistent with the lack of the correlation between the observed hot gas temperature and K-band luminosity of galaxies. The simulated coronae typically represent subsonic outflows, chiefly because of the semi-confinement. As a result, the hot gas density increases with the ICM thermal pressure. The ram pressure, on the other hand, chiefly affects the size and lopsidedness of the coronae. The density increase could lead to the compression of cool gas clouds, if present, and hence the formation of stars. The increase also enhances radiative cooling of the hot gas, which may fuel central supermassive black holes, explaining the higher frequency of active galactic nuclei observed in clusters than in the field. The radiation enhancement is consistent with a substantially higher surface brightness of the X-ray emission detected from coronae in cluster environment. The total X-ray luminosity of a corona, however, depends on the relative importance of the surrounding thermal and ram pressures. These environment dependences should at least partly explain the large dispersion in the observed diffuse X-ray luminosities of spheroids with similar stellar properties. Furthermore, we show that an outflow powered by the distributed feedback can naturally produce a positive radial gradient in the hot gas entropy, mimicking a cooling flow.

Key words: method: numerical ISM: kinematics and dynamics X-ray: galaxies: clusters

1 INTRODUCTION

Though consisting of primarily old stars, galactic spheroids (bulges of Sb-Sa spirals as well as S0 and elliptical galaxies) are a major source of stellar feedback in form of mass loss and Type Ia supernovae (e.g., Ciotti et al. 1991; Knapp et al. 1992; Mannucci et al. 2004). The specific energy of this feedback predicts that it should present primarily in X-ray-emitting hot gas. Indeed, such hot gas has been detected in and around spheroids, which typically contain little cool gas. However, it has been shown repeatedly that the X-ray-inferred hot gas mass and energy are far less than the empirical predictions from the feedback inputs (e.g., David et al. 2006; Li et al. 2006; Li and Wang 2007; Li et al. 2007; Wang 2010). This missing stellar feedback has most likely escaped into large-scale galactic halos, where the gas becomes too tenuous to be detected in existing X-ray imaging observations (e.g., Tang et al. 2009a and references therein). The implication of this scenario is profound, because the injection of the mass and energy into the halos could strongly affect the ecosystem of the galaxies and hence their evolution (Tang et al. 2009a).

While the above qualitative picture seems clear, there are key issues that still need to be addressed to understand both the stellar feedback itself and its interplay with the environment. Significant uncertainties are still present in the mass and energy input rates of stars (§ 2). The energy input rate is inferred from observations of SNe in a large sample of galaxies of diverse optical and near-IR luminosities as well as types (e.g., Mannucci et al. 2005), assuming a certain explosion mechanical energy deposited into the interstellar space. The stellar mass loss rate is based on the modeling of the 12 μm emission from the circumstellar medium of evolved stars (e.g., Knapp et al. 1992). These

⋆ E-mail:lv@astro.umass.edu

semi-empirical rates, uncertain by a factor of at least ~ 2 for individual galaxies, can in principle be directly constrained by the measured temperature and luminosity of galactic coronae. Indeed, detailed simulations have been conducted for relatively isolated "field" spheroids and have been compared with observations (Tang et al. 2009a,b; Tang & Wang 2010), which have led to a qualitative understanding of the feedback processes and effects on X-ray measurements. In particular, the feedback model expects that the specific energy should not change substantially from one spheroid to another, which is consistent with little correlation between the measured temperatures and K-band luminosities L_K (e.g., David et al. 2006; Sun et al. 2007). But the measured temperatures ($\lesssim$ 1 keV) are substantially lower than the expected value from simulations. The measured iron abundances of coronal gas are also typically lower than expected for the Ia SN-enriched gas (§ 2). At least part of these discrepancies can be accounted for by various 3-D effects of the Ia SN heating, which produces very low-density, hot, fast-moving, and enriched bubbles that hardly radiate. When the gas in these bubbles finally mixed with the material from the stellar mass loss at large radii, the X-ray emission becomes too weak and diffuse to be effectively detected (Tang et al. 2009a,b; Tang & Wang 2010). The observed X-ray emission thus gives only a biased view of the coronae. We expect that this bias should be minimal for a corona in the ICM, however. The high external thermal and ram pressures tightly confine such coronae, resulting in a low outflow speed and hence relatively local mixing of the feedback materials. Furthermore, one can better characterize the ICM environment from observations, important for a self-consistent modeling of a corona. Therefore, coronae embedded in the ICM are ideal sites to better constrain the feedback and its interplay with the environment.

There have also been significant efforts in studying stellar feedback-powered coronae embedded in the ICM, mostly focusing on the ram-pressure stripping of hot gas (e.g., Acreman et al. 2003; Stevens et al. 1999; Toniazzo & Schindler 2001). It is shown that the global morphological and integrated properties, such as gas mass and luminosity, are strongly influenced by the environment. A set of 2D simulations done by Stevens et al. (1999) show that galactic coronae can be maintained by stellar feedback in poor clusters while be efficiently stripped in rich ones. Acreman et al. (2003) and Toniazzo & Schindler (2001) simulated galaxies falling into clusters and demonstrated that a galactic corona reached a cyclic "stripping replenishment" dynamics due to the periodic orbital motion of the host galaxy as well as the competing processes such as stripping and stellar feedback.

We focus on modeling coronae in and around intermediate-mass spheroids that are embedded in the ICM. Such a system is relatively simple with minimum effects due to the feedback from AGNs and to the radiative cooling of hot gas. We expect that the hot gas is in a quasi-steady, subsonic outflow semi-confined by the thermal and ram-pressures of the ICM. This state should be only sensitive to the local properties of the ICM (see § 2 for more discussion), avoiding large uncertainties in modeling the history of the galactic feedback and the evolution of the environment, as would be needed for a field spheroid (Tang et al. 2009a). The simulations can also be compared with an increasing number of X-ray detections of galactic coronae of such spheroids (e.g., Sun et al. 2007), leading to an improved understanding of the feedback itself and its interplay with the environment. In particular, we examine the dependence of the corona properties on the specific energy of the stellar feedback and on the thermal and ram pressures of the ICM and check how measurements (e.g., temperature, surface brightness, overall luminosity and morphology) may be made to infer the parameters that cannot directly observed (e.g., the ICM thermal and ram pressures local to an individual galaxy). Here, we will present 2-D simulations only, which allow for an efficient exploration of a large parameter space. The paper is organized as follows: We briefly describe our numerical model and setup in § 2 and present results in § 3; We discuss their implications in § 4; Finally in § 5, we summarize our conclusions.

2 MODEL AND SIMULATION SETUP

2.1 Model Galaxies

Our model galaxy is composed of a stellar spheroid component and a dark matter halo. We use the spherical Hernquist density profile (Hernquist 1990) to represent the stellar mass distribution:

$$\rho_s(r) = \frac{M_s}{2\pi a^3}\frac{a^4}{r(r+a)^3}, \tag{1}$$

where M_s is the total stellar mass, and a is the scale radius. This density profile results in a gravitational potential

$$\phi(r) = -\frac{GM}{(r+a)}. \tag{2}$$

The above stellar mass distribution resembles the de Vaucouleur's Law; The relation between the half-light radius R_e and the scale radius is $R_e = 1.8513a$.

We characterize the dark matter halo with the NFW profile (Navarro et al. 1997),

$$\rho_d(r) = \frac{\rho_0}{(r/r_d)(1+r/r_d)^2}, \tag{3}$$

where r_d is the scale radius of the dark halo, and ρ_0 is defined as

$$\rho_0 = \frac{1}{3}\rho_{crit}\Omega_m\Delta_{vir}\frac{c^3}{\ln(1+c) - \frac{c}{(1+c)}}, \tag{4}$$

in which ρ_{crit} is the critical density of the universe. The dark halo has a mass M_{vir} within the virial radius r_{vir}, which is defined to have a density that is Δ_{vir} times the mean matter density of the universe $\rho_{crit}\Omega_m$. We adopt Δ_{vir} to be 250. Therefore, we have the relation

$$M_{vir} = \frac{4\pi}{3}r_{vir}^3\Delta_{vir}\rho_{crit}\Omega_m, \tag{5}$$

where c is the concentration factor defined as $c = \frac{r_{vir}}{r_d}$ and is related to M_{vir}. We set $c = 13$ (Eke et al. 2001). Thus, for a given cosmology and a given M_{vir}, the mass profile of the dark halo is totally determined.

2.2 Stellar Feedback

The stellar mass and energy feedback in spheroids are dominated by the mass loss and Ia SNe of evolved stars, respec-

tively. We neglect the energy input from the random motion of stars and hence their ejecta. The total energy released by type Ia SNe is

$$\dot{E} = E_{SN} n_{SN} \Big(\frac{L_K}{10^{10} L_{K,\odot}} \Big), \tag{6}$$

where $n_{SN} = 0.00035$ yr^{-1} for E/S0 galaxies according to Mannucci et al. (2005). The empirical mass input rate from the stellar mass loss is

$$\dot{M} = m \Big(\frac{L_K}{10^{10} L_{K,\odot}} \Big), \tag{7}$$

where $m = 0.021$ M$_\odot$yr^{-1} according to Knapp et al. (1992). Assuming that the mechanical energy of each SN is 10^{51} erg, the specific energy of stellar feedback is $\beta = \frac{\dot{E}}{\dot{M}} \sim 5$ keV per particle. To account for the uncertainties in these rates and assumptions, we also sample three different lower values of the specfic energy for comparison with observations (Table 1). We assume that the energy and mass inputs follow the distribution of the stellar mass.

In addition, each Ia SN produces $\sim 0.7 M_\odot$ of iron ejecta. We assume that the iron abundance of the mass loss from stars is solar. If the ejecta is fully and instantaneously mixed with the mass loss, the expected iron abundance relative to the solar value is then

$$\Big(\frac{n_{sn} M_{Fe}}{m} \Big) / Z_\odot \sim \Big(\frac{0.0018 \times 0.7 M_\odot}{0.2 M_\odot} \Big) / Z_\odot = 5.5. \tag{8}$$

However, in observations, supersolar metallicity is quite rare. Tang et al. (2009b) and Tang & Wang (2010) have shown that Ia SN ejecta may not be efficiently mixed with stellar mass loss on microscopic scale, resulting in a low effective metallicity of the ISM. While our focus is on the environmental effect. In our simulation, we set the iron abundance of the input mass to the solar value.

2.3 Simulation Setup

The gas hydrodynamics and metal abundance distribution with both the stellar feedback and radiative cooling can be described by the following equations:

$$\begin{aligned}
\frac{\partial \rho_g}{\partial t} + \nabla \cdot (\rho_g \mathbf{v}) &= S_m \\
\frac{\partial (\rho_g \mathbf{v})}{\partial t} + \nabla \cdot (\rho_g \mathbf{v}\mathbf{v} + P[I]) &= \rho_g \mathbf{g} \\
\frac{\partial (\rho_g e)}{\partial t} + \nabla \cdot [(\rho_g e + P)\mathbf{v}] &= S_e - n_e n_i \Lambda(T, Z) + \rho_g \mathbf{g} \cdot \mathbf{v} \\
\frac{\partial (\rho_g X_{iron})}{\partial t} + \nabla \cdot (\rho_g X_{iron} \mathbf{v}) &= S_{iron}.
\end{aligned} \tag{9}$$

The first equation is mass conservation law, with ρ_g denoting the mass density of the coronal gas. The second is momentum equation. P is gas pressure and $\mathbf{g}$ is gravitational acceleration. The third one is energy equation. e stands for the specific energy of the gas, including both thermal and kinetic components. The second term to the right is cooling rate. We adopt the cooling curve from Sutherland & Dopita (1993), assuming an optically-thin thermal plasma in collisional ionization equilibrium. For calculation of the radiation in a specific band, we use the Mekal model, extracted from the X-ray spectral analysis software XSPEC. We use the fourth equation to keep track on the iron mass fraction, which is denoted by X_{iron}.

We conduct our simulations with the FLASH code (Fryxell et al. 2000), an Eulerian astrophysical hydrodynamics code with the adaptive mesh refinement (AMR) capability. The simulated region is fixed in the galaxy-rest frame using cylindrical coordinates, with z ranging from -50 kpc to 50 kpc and the radius from 0 to 50 kpc. The axis of the cylinder is through the center of a simulated spheroid and along the direction of its motion. The upper and lower boundary conditions are fixed so that the ICM flows in and out the simulation region at a constant speed. This mimics the motion of galaxies through a local cluster environment. We apply reflection boundary condition at $r = 0$ and diode boundary condition, which only allows gas to flow out, to the right side of the simulation region. Compared with the simulation box, which is 50 kpc by 100 kpc, the coronae are only on the order of 1 kpc to 10 kpc across. Data near the outer regions will be excluded in our analysis to avoid any potential artifacts introduced by the assumed outer boundary condition of the simulations. Also, the outer region will not be shown in the following images. We allow the resolution to reach 0.1 kpc, so that the small coronae can be well resolved.

When a simulation starts, there is no interstellar gas in the galaxy. As the simulation progresses, the stellar feedback gradually accumulates in and around the spheroid to form a corona, which is characterized by its higher iron abundance. In the mean time, the ram-pressure and turbulent motion strips gas at the outer boundaries of the corona. We end the simulation when it reaches a statistically quasi-steady state. Empirically, the time to reach such a state is $\tau_g \sim 0.2$ Gyr, while the time for the ICM to pass the simulation region ranges from 0.05 Gyr to 0.2 Gyr. Representative results are all extracted from the simulations after this time.

The presence of a local quasi-steady state is a reasonable assumption for a compact corona. As a galaxy moves through a cluster, the ICM condition can of course change drastically. But the time scale for such a change is typically much longer than the dynamic time for the corona to adapt the local environment. For a cluster of a characteristic size of ~ 1 Mpc and temperature of 2 keV, for example, the crossing time for a galaxy moving roughly at the sound speed is $\tau_{c1} \sim 2$ Gyr. In contrast, for a corona of a typical size ~ 5 kpc and temperature ~ 0.8 keV, the sound crossing time is only $\tau_{c2} \sim 20$ Myr. Even if a corona is totally destroyed at some point(e.g. at the central region of a cluster), the re-building time scale τ_g, as dicussed above, is still shorter than the environment change time scale. Therefore, the local quasi-steady state is a reasonable assumption for characterizating the environmental impact on galactic coronae.

3 RESULTS

We have simulated a set of cases to characterize the dependence on key parameters. Table 1 lists our adopted model parameter values. The different combinations of the ICM density (n_i, the number density of all particles) and temperature (T_j) as well as the Mach number ($\mathcal{M}_k$) and specific energy (β_l) of the model galaxy form a set of 48 cases.

Here we present the gas properties extracted from the simulations. We first detail the results for a representative

Table 1. Model Parameters

Model galaxy	Stellar Mass(10^{11} $M_\odot$)	2.0
	Dark Halo Mass (10^{11} $M_\odot$)	40
ICM properties	ICM density (10^{-4} cm^{-3})	3.3(n_1), 10(n_2)
	ICM temperature (10^7 K)	2.0(T_1), 6.0(T_2)
	Iron abundance ($Z_\odot$)	0.3
	Mach number	0.6($\mathcal{M}_1$), 1.2($\mathcal{M}_2$), 1.8($\mathcal{M}_3$)
Stellar feedback	Mass loss rate ($M_\odot/10^{11}$ $M_\odot$/yr)	0.32
	Specific energy (keV)	1.2(β_1), 1.8(β_2), 3.0(β_3), 4.8(β_4)
	Iron abundance ($Z_\odot$)	1.0

case $n_1T_2\mathcal{M}_2\beta_2$ (§ 3.1) and then discuss the similarity and significant variation among the different cases (§ 3.2).

3.1 Representative Case

Fig. 1 shows a snapshot of the representative simulation case $n_1T_2\mathcal{M}_2\beta_2$ in terms of the Mach number, thermal pressure, density, and temperature distributions. At the very front of the corona is a smooth and distinct boundary that separates the corona from the ambient medium. This is a contact discontinuity, across which the density, temperature and metallicity change abruptly. Compared to the surrounding medium, the corona is cooler and denser. The iron abundance inside the corona is a constant which is equal to the value of injected material (Fig. 2). Outside the corona the abundance drops rapidly to the value of the ICM, although it is contaminated by the local stellar feedback. Therefore, we can use the abundance to trace the morphology of the corona gas. Inside the corona, the Mach number of the gas flow is so low (~ 0.1) that it is almost hydrostatic (see § 4.1).

While the main body of a corona can reach a nearly steady state, both the interface with the surrounding ICM and the tail are unstable. The individual features in these later parts can strongly fluctuate with time. The side horns are characteristic sign of the Kelvin-Helmholtz (KH) instability. As a result, the corona gas is torn off and pushed back to form a chaotic tail. Therefore, the stripping is primarily due to the hydrodynamic instability rather than the ram-pressure itself. Similarly, the instability also leads to the dynamic mixing of the corona gas with the ICM, although numerically this is achieved on the spacial scale of the simulation resolution.

Fig. 3 shows the 1-D distribution of the iron abundance, density, temperature and entropy of the corona along the z axis of the simulation box. Here the entropy is defined as $S = \frac{T}{n^{\gamma-1}}$ (γ is the specific heat ratio of the gas and is equal to $\frac{5}{3}$). The distributions are averaged over a time span of 50 Myr when the simulation has reached a quasi-steady state.

While the gas density drops substantially from the center of the spheroid to the outer outskirt of the corona, the temperature does not change much (Fig. 3). The specific energy of the feedback determines the specific enthalpy of the corona gas and therefore the temperature ($T = \frac{\beta}{2.5k_B}$) when the radiative cooling is not important as in the present case. The small drop of the temperature towards the outskirt (by a factor of up to 1.2) is largely due to the outflow that needs to climb out of the gravity potential. But, because of the distributed nature of the mass and energy injection, the drop

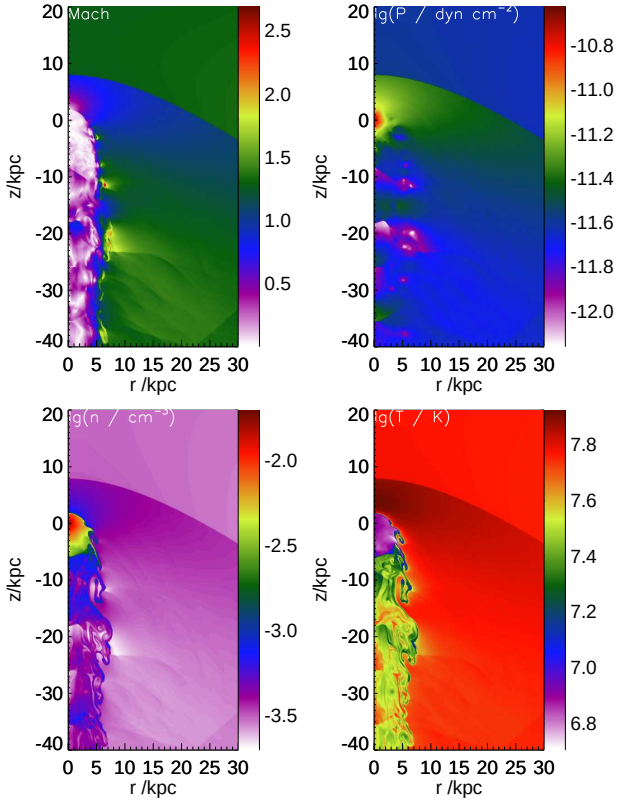

Figure 1. Model $n_1T_2\mathcal{M}_2\beta_2$ seen in the Mach number, thermal pressure, density, and temperature.

is much smaller than what is predicted from the Bernoulli's law for ideal gas moving from the center to the outskirt.

Another interesting characteristic of the simulated corona is the positive radial entropy gradient. This is apparently caused by the nearly constant temperature profile and the steep density drop from the center to the outskirts, as required to maintain a nearly hydrostatic state of the corona (§ 4.1). Physically this positive entropy gradient is a natural result of an outflow that is continuously heated by the stars along the way out.

3.2 Similarity and Variance among the Cases

Here we focus on the similarity and significant variance in the hot gas properties of the various simulated cases, in reference to the representative one ($n_1T_2\mathcal{M}_2\beta_2$) detailed above.

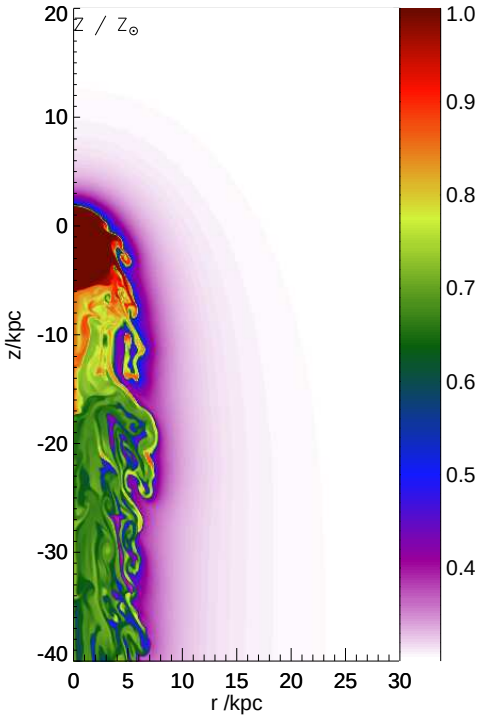

Figure 2. Iron abundance map for model $n_1T_2\mathcal{M}_2\beta_2$.

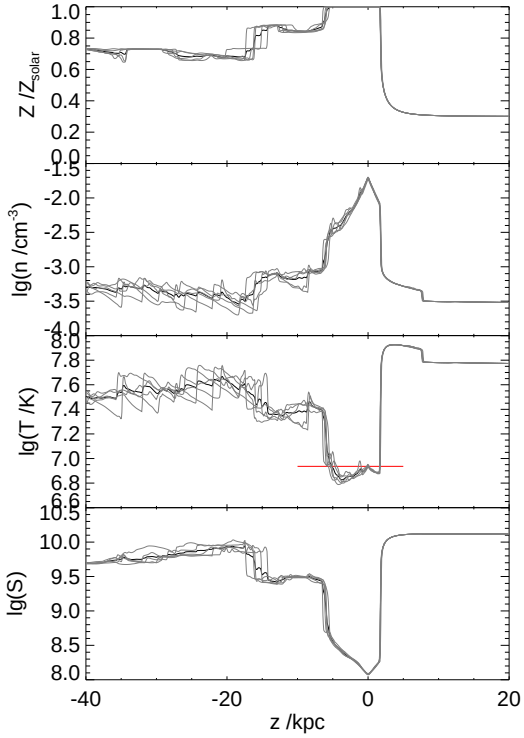

Figure 3. Iron abundance, denisty, temperature, and entropy distributions along z-axis of the simulation of case $n_1T_2\mathcal{M}_2\beta_2$. The thick solid lines are time-averaged profiles over a time span from 250 to 300 Myr (the residual wigglers are present due the the limited number of snapshots used in averaging), while the thin lines are extracted from several snapshots. The horizontal red line in the temperature panel corresponds to $T = \frac{\beta}{2.5k_B}$.

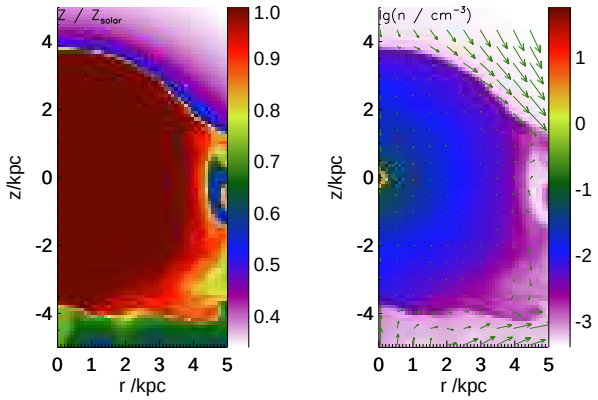

Figure 4. Iron abundance and density distributions in the $n_1T_2\mathcal{M}_1\beta_1$ case. The arrows represent the velocity field. Note the central density peak (the red spot) at the very center.

In most of the simulation cases, the coronae are clearly in the outflow state. The radiative cooling is not important, except for some such as $n_2T_1\mathcal{M}_1\beta_1$, $n_2T_1\mathcal{M}_2\beta_1$, $n_1T_2\mathcal{M}_1\beta_1$, $n_2T_2\mathcal{M}_1\beta_1$ and $n_2T_2\mathcal{M}_2\beta_1$, with combination of low specific energy and high ICM pressure. The gas at the spheroid center is so dense that an inward cooling flow is developed in the inner region. (Fig. 4). Such cooling flows, commonly seen in similar models and simulations, may naturally induce activities of the central supermassive black holes. The feedback from such activities has been proposed to substantially reduce the net cooling (e.g. Mathews & Brighenti 2003; Fabian & Sanders 2009). While a study of this topic is beyond the scope of the present work, we here keep our focus on discussing the morphological and physical properties of the outflow cases, which probably represent more typical cases of galactic coronae in the ICM.

For all the $n_2T_2\mathcal{M}_3$ cases, coronae fail to form due to the high thermal and ram pressures, leaving only a track with high iron abundance (Fig. 5). In each of these cases, the density peaks away from the spheroid center.

Fig. 6 show outlines of the coronae. These outlines are represented by the iso-abundance contours of the value of $Z_\odot$, or approximately the contact discontinuity between corona gas purely ejected by the spheriods and the ICM. The characteristic size of a corona is sensitive to the thermal pressure of the surrounding ICM as can be seen in panel (a) of Fig. 6. The corona in the ICM of n_1T_1, which is typical of a group or poor cluster, is more than 10kpc across, while the corona in the ICM of n_2T_2, which is typical of the core region of a relatively rich cluster, is less than 3kpc across. The motion of the host galaxy relative to the surrounding medium, which is represented by the Mach number, mainly influences lopsidedness of a corona. In the subsonic case, the corona is almost spherical, while in the supersonic case with the Mach number as high as 1.8, the corona is significantly narrowed and elongated. As the input energy of the stellar feedback increases, the lopsidedness increases. This is not surprising. As the stellar feedback becomes more energetic, the density of the corona gas will be lower. As a result, the gravitational restoring force become less important, compared with the ram pressure.

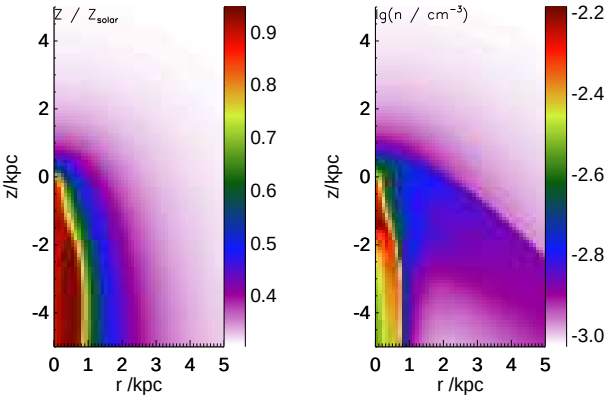

Figure 5. Iron abundance and density distributions in the $n_1T_2\mathcal{M}_1\beta_1$ case, in which the corona fails to form.

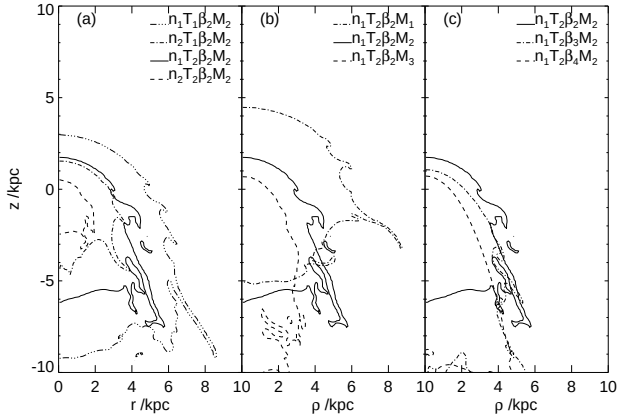

Figure 6. Outlines of the simulated coronae. The outline for each case is defined to be the contour of the iron abundance equal to $Z_\odot$. The reference model $n_1T_2\mathcal{M}_2\beta_2$ is represented with solid line in all the three figures. Panels (a), (b) and (c) correspond to variation in nT, Mach number and β, respectively, illustrating how the coronae respond to the changes of the surrounding environment and stellar feedback.

The dependence of the corona temperature on the specific energy of injected material can be clearly seen in Fig. 7. The peak value of the corona temperature is always roughly $\frac{\beta}{2.5k_B}$; it drops slightly outwards largely due to the presence of gravitational potential as described in § 3.1.

We plot the peak density values of the coronae in Fig. 8 and selected density profile along the z-axis in Fig. 9, illustrating how the coronae respond to the changes of surrounding environment and inner stellar feedback. Generally, the corona density depends strongly on the thermal pressure of the surrounding medium, but only weakly on the ram pressure. In our simulation, the the Mach number ranges from 0.6 to 1.8, with the ratio between the largest ram pressure and the smallest one as high as 9, the corona density changes slightly except for case $n_2T_2\mathcal{M}_1\beta_2$ and its high Mach number version $n_2T_2\mathcal{M}_2\beta_2$. This makes sense because unlike thermal pressure, which compresses a corona from all directions, ram-pressure only acts on the front side and therefore mostly pushes the gas backwards rather than compressing it. The coronae in cases of n_2T_1 are compressed more than those in cases of n_1T_2, although the ICM thermal pressure

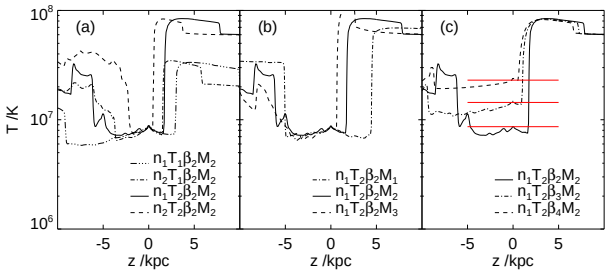

Figure 7. Temperature profiles along z-axis. The red horizontal lines in (c) represent $\frac{\beta}{2.5k_B}$. The reference model $n_1T_2\mathcal{M}_2\beta_2$ is represented with solid line in all the three figures. Panels (a), (b) and (c) correspond to variation in nT, Mach number and β respectively, illustrating how the coronae respond to the changes of the surrounding environment and stellar feedback.

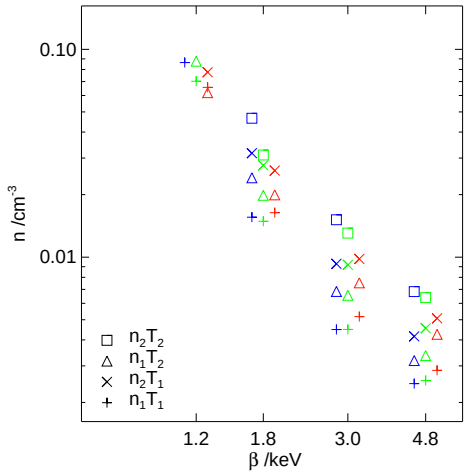

Figure 8. Peak density values of the coronae. Cases with central cooling flow and those in which the coronae fail to form are not shown. Cases with different ICM thermal states are represented with different symbols, while different Mach numbers are coded in different colors with red for 1.8, green for 1.2 and blue for 0.6. To avoid overlap among the symbols, the higher Mach number models are shifted to the right a litte bit and the subsonic cases to the left.

is the same. This is caused by larger focusing effect of gravitational force of the galaxy on the ICM with lower temperature.

Fig. 10 includes the luminosity of each simulated corona in the $0.3-2.0$ keV X-ray band. For simplicity, we use the iron abundance distribution to define the shape of a corona as what we do to plot the outline of a corona. Every grid point with iron abundance equal to the solar value is included to measure the luminosity. The emissivity is a function that depends on both temperature and metallicity. If we assume the metals, mostly iron, produced by Ia SNe, are fully mixed in the corona gas, the total luminosity would be enhanced by a factor of about 3. It is clear that the luminosity decreases with the increasing Mach number and/or β. But the dependence on the ICM thermal pressure is not that simple: the luminosity tends to increase with the pressure in

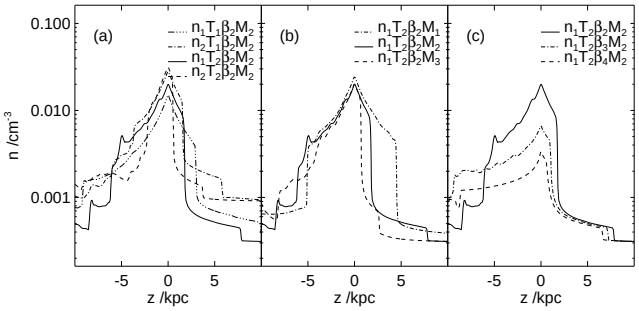

Figure 9. Density profiles along z axis. The reference model $n_1T_2\mathcal{M}_2\beta_2$ is represented with the solid lines. Panels (a), (b) and (c) show the dependence on nT, Mach number, and β, respectively.

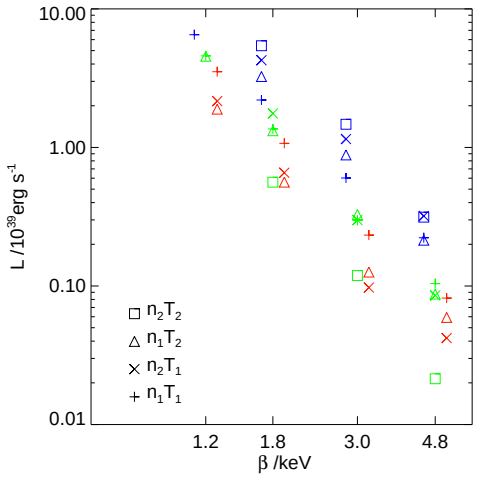

Figure 10. Luminosity of the coronae. Cases with central cooling flow and those in which the coronae fail to form are not shown. Cases with different ICM thermal states are represented with different symbols, while different Mach numbers are coded in different colors with red for 1.8, green for 1.2 and blue for 0.6. To avoid overlap among the symbols, the higher Mach number models are shifted to the right a litte bit and the subsonic cases to the left.

subsonic cases (lower Mach numbers), while the trend goes in the opposite direction in the supersonic cases.

4 DISCUSSION

The above results give a basic characterization of galactic coronae powered by stellar feedback and semi-confined by the thermal and ram prssures of the ICM. In this section, we first give a physical account of the apparent ICM impacts on the corona characteristics as described above, then compare the results with observations to constrain the stellar feedback, and finally discuss the implications for other galactic properties.

Table 2. α for various cases.

	β_1	β_2	β_3	β_4
n_1, T_1	0.99	1.47	2.30	3.33
n_2, T_1	0.33	0.49	0.77	1.11
n_1, T_2	0.33	0.49	0.77	1.11
n_2, T_2	0.11	0.16	0.25	0.37

4.1 ICM Impacts on the Coronae

The properties of a corona are affected by several competing processes, the stellar feedback, the galaxy gravitational attraction, and the thermal/ram pressures of the ICM. In the simplest case, when the gravity and external pressure can be neglected, the density at the center would then be determined entirely by the mass/energy injection. In this case, we can define a characteristic density as

$$\rho_{c,1} = \frac{3}{4\pi}\frac{\dot{M}}{a^3}\tau. \tag{10}$$

Here $\tau = \frac{a}{c_s}$ is the dynamic time scale of the corona, where c_s is the sound speed. Considering that the temperature is determined by the specific energy β, the characterisitic value of the pressure is

$$P_{c,1} = \frac{3}{4\pi}\frac{\dot{M}}{a^2}\frac{\sqrt{(\gamma-1)\beta}}{\gamma}. \tag{11}$$

In the other extreme, when the gravity is important (i.e., the corona is nearly hydrostatic), the Mach number of the outflow must be low. Clearly, in this case, the external thermal pressure becomes important as well. Because the corona is nearly isothermal, the pressure distribution is

$$\ln(P) = \ln(P_0) - \frac{\mu m_p(\Phi-\Phi_0)}{k_B T}, \tag{12}$$

where P_0 is the pressure at the outer boundary and $\Phi - \Phi_0$ is the gravitational potential difference. Assuming that the corona size is considerably larger than the scale a of the stellar spheroid, we obtain a characteristic peak pressure as

$$P_{c,2} = P_{ICM}\exp\left(\frac{GM_s}{a}\sqrt{\frac{\gamma}{(\gamma-1)\beta}}\right). \tag{13}$$

To characterize the relative importance of the feedback to the gravity, we define a dimensionless parameter as

$$\alpha = \frac{P_{c,1}}{P_{c,2}}. \tag{14}$$

The values of this parameter for the simulated cases are listed in Table.2. Fig. 11 compares the hydrostatic solutions (Eq. 13) to the simulations with three different α parameters. In those cases with small α, such as $n_2T_2\mathcal{M}_1\beta_2$, in which the gravity dominates over the feedback, the hydrostatic solutions give nearly perfect matchs to the simulated pressure profiles. While in a case like $n_1T_1\mathcal{M}_1\beta_4$ (with $\alpha = 3.3$), where the feedback dominates, the deviation of the hydrostatic solution from the simulated profile is apparent. For the cases which we think are plausible (β=1.8keV, see § 4.2), α is about 1.0 or much less than 1.0, and the coronae are largely in hydrostatic state.

Although the same model galaxy (in terms of the stellar and dark matter masses) is adopted for all the simulation

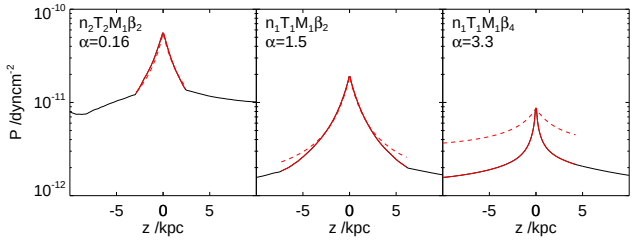

Figure 11. Comparison between numerical pressure profiles and the theoretical profiles with isothermal assumption. The solid lines are the pressure profiles extracted from the simulations and the dashed lines represent the corresponding hydrostatic solutions. The region inside the coronae is colored in red. In each of the panels, the peaks of both of the numerical profile and theoretical one are positioned at the same point.

cases, the resultant X-ray luminosities can still differ by up to two orders of magnitude, due to the different choices of the Mach number, β, and/or thermal pressure values of the ICM. Because the corona temperature is determined by β, the gas density is

$$n_c \sim \frac{P_{ICM}}{\beta}, \tag{15}$$

if the corona is in a nearly hydrostatic state. Therefore, the surface brightness of a corona provides a measure of the ambient ICM pressure and thus may be used to estimate the line-of-sight position in a cluster.

However, the X-ray luminosity of a corona depends on several factors. Fig. 10 shows a clear anti-correlation between the luminosity and specific energy β. This anti-correlation is primarily due to the density decrease with the increase of β, although it does not strongly affect the size of a corona. The ICM thermal pressure tends to squeeze the corona, hence enhance its luminosity (subsonic cases). But this effect is complicated by the presence of the ram-pressure. As the Mach number increases, the lumonosity can decrease because the ram-pressure stripping reduces the overall size ofthe corona. These dependences on the environment as well as the stellar feedback energetics may naturally explain the observed large dispersion of L_x/L_K for spheroids of similar L_K. The complications in the dependences may also account for the lack of a clear observed trend in the ICM environment effect on X-ray luminosities of coronae (Sun et al. 2007; Mulchaey & Jeltema 2010).

4.2 Implication for the Feedback Model

In our model of the galactic coronae, the gas temperature is primarily determined by the specific energy of the stellar feedback and thus should not change significantly with the stellar mass. This independence on the mass or L_K is consistent with the temperature measurements of the coronae of intermediate-mass spheroids (David et al. 2006; Sun et al. 2007; Jeltema et al. 2008; Boroson et al. 2010). This is in contrast to the correlation between the temperature and L_B for more massive systems such as clusters and groups of galaxies (Helsdon & Ponman 2003). In particular, galaxy clusters show a well-defined scaling law between the temperature and luminosity of the observed hot gas, which is a natural result of the predominant gravitational heating in the self-similar cluster formation. The scaling law for lower mass systems (e.g., groups of galaxies) is known to be slightly different from that for clusters (e.g., showing an 'entropy floor'), which is believed to be an imprint of preheating(e.g., starburst and early AGNs). Correlation between L_B and the temperature of hot gas is observed in massive X-ray-bright elliptical galaxies, especially for central galaxies in groups and clusters (e.g,, O'Sullivan et al. 2003). But the entropies are found lie below the entropy floor($\sim 10^9$ K cm^{-2}) discovered in groups of galaxies. Radiative cooling could account for the low entropy, although how this runaway process may be balanced by the heating due to the mechanical inputs from both stellar and AGN feedbacks remains unclear. We have shown that the low value and the positive radial gradient of the entropy are expected from the distributed feedback in intermediate-mass spheroids, in which the radiative cooling is not important. Therefore, we may conclude that the coronae of intermediate-mass spheroids represent the extreme case in which the stellar feedback plays a dominant role, which means they are produced by stellar mass loss and heated by SNe.

We may further constrain the stellar feedback based on the measured temperature of the coronae. Though with a relative large dispersion, the measured temperatures are mostly fall in the range of $0.5 - 1.0$ keV, which is significantly higher than those measured in field spheroids, but is still substantially lower than what is inferred from our 2-D simulations if the canonical specific energy value of the stellar feedback is assumed (~ 5 keV; see § 2). Part of this discrepancy could still be due to the 3-D effects of discrete heating by Ia SNe, as mentioned in § 1 (and characterized in Tang et al. 2009b; Tang & Wang 2010). But we expect that such effect should be substantially weaker in the compact coronae embedded in the high pressure ICM and that the measured temperature should more faithfully reflect the specific energy of the feedback. To match the measured temperature range of the coronae requires a specfic energy of $\sim 1.5 - 3$ keV, or a factor of $\sim 2 - 3$ lower than the canonical value (5 keV; § 2). This factor is probably still within the uncertainties of the semi-emipirical mass and energy injection rates. Further, the assumed mechanical energy per Ia SN could be somewhat (e.g., a factor of ~ 2) less than 10^{51} ergs. Also a considerable fraction of the energy can be used to generate cosmic rays, magnetic field and turbulent motion. The diversion of the energy into these various forms could significantly reduces the temperature, although the hydrodynamics of the coronae, hence the density and pressure distributions, should not be significantly affected. The simulated coronae with $\beta = 1.8$ keV generally have individual luminosties of a few times 10^{39} erg s^{-1}, consistent with the observed range of $10^{39} \sim 10^{40}$ erg s^{-1} (Sun et al. 2007). A considerably large value of β is not favored, because it decreases the expected luminosity steeply (Fig. 10).

4.3 Implifications for Understanding Other Galactic Components

We discuss here the potential impacts of the pressure or density enhancement of the coronae on the fueling of the central SMBHs and the evolution of cool gas, if present in the spheroids.

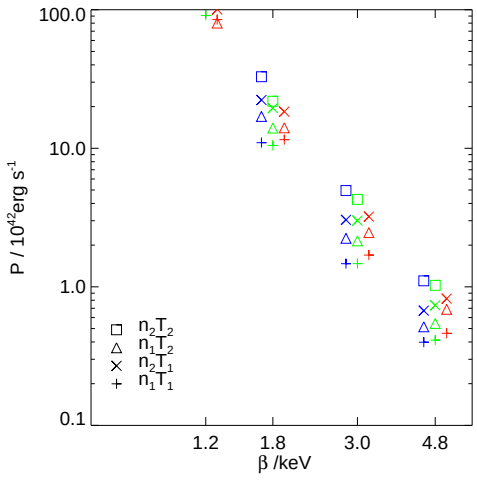

Figure 12. Estimated AGN power. Cases with cooling flow and those in which the coronae fail to form are not shown. Different ICM thermal states are represented with different symbols and different Mach numbers are coded in different colors with red for 1.8, green for 1.2 and blue for 0.6. To avoid overlap among the symbols, the higher Mach number models are shifted to the right a litte bit and the subsonic cases to the left.

The simulation shows that the central density of a corona is sensitive to the thermal pressure of the surrounding medium. To infer the power of a SMBH, we adopt the Bondi accretion rate (Edgar 2004):

$$\dot{M} = \frac{4\pi G^2 M_{BH}^2 \rho}{c_s^3}. \quad (16)$$

where M_{BH} is the mass of the SMBH, while ρ and c_s are the density and sound speed at the center of a corona. Assuming the fraction of the accretion energy released is $\eta = 0.1$, the power of the SMBH can be approximated as

$$2.12{\times}10^{41}\ \mathrm{erg\ s^{-1}} \left(\frac{M_{BH}}{10^8\ \mathrm{M_\odot}}\right)^2 \left(\frac{n}{\mathrm{cm^{-3}}}\right) \left(\frac{T}{7.0\times10^7\ \mathrm{K}}\right)^{-1.5} \quad (17)$$

The SMBH mass can be estimated from its correlation with the spheroid mass $M_{BH} \sim 0.006 M_{bulge}$ (Magorrian et al. 1998). Fig. 12 shows the dependence of the power on the ICM state, the Mach number of spheroid, and the specific energy of the feedback.

In particular the luminosity for the most plausible β_2 cases is about 10^{43} erg s^{-1}, which falls in the range of the X-ray power of a low luminosity AGN. This indicates that a compact corona built up by stellar feedback and embedded in cluster environment could feed a moderate AGN. The ICM pressure also tends to enhance the accretion, consistent with the finding that the galaxies with $L_x > 10^{42}$ erg s^{-1} AGNs are more centrally concentrated than ones without (Martini et al. 2007). These galaxies with AGNs are not dominated by galaxies that have recently entered the clusters. Similar conclusions are also reached in more recent studies, such as the one by Hart et al. (2009), based on the analysis of a sample of $P_{1.4GHz} > 3\times10^{23}$ WHz^{-1} radio galaxies and $L_{0.3-8keV} > 10^{42}$ erg s^{-1} point sources.

The pressure enhancement could also have significant impacts on cool gas in a galaxy. Under high pressure, cool gas exists preferentially in molecular form rather than atomic one. The compression of cold gas because of the ICM pressure could further lead to star formation (Bekki & Couch 2003), depriving the galaxy of the gas further. Thus it is expected that galaxies contain less amounts of cool gas in clusters than in the field. These impacts should affect cool gas not only in spheroids, but in spirals as well, consistent with existing observations (Young & Scoville 1991).

5 SUMMARY

We have conducted a range of 2-D hydrodynamic simulations of galactic coronae that result from gradual energy and mass feedback in stellar spheroids moving in the ICM enviornment. We have focused on spheroids that are in the intermediate-mass range (corresponding to $L_K \sim 10^{11} - 10^{12} L_{K,\odot}$) so that both the AGN feedback and the radiative cooling of the hot gas could largely be neglected. We explore the dependence of corona properties on the specific energy of the stellar feedback as well as on the ram and thermal pressures of the ICM. Our major results and conclusions are as follows:

(i) X-ray coronae embedded in clusters could be naturally explained by the subsonic outflow driven by the stellar feedback, semi-confined by the ram-pressure and compressed by thermal pressure of the surrounding ICM. The corona temperature depends primarily on the specific energy of the input material in such a way that $T \sim \frac{\beta}{2.5k_B}$. The decrease of the thermal energy due to the climbing of the gravitational potential and the expansion is largely compensated by the distributed heating by Ia SNe. This result naturally explains the lack of the correlation between the temperature and K-band luminosity for the spheroids in our considered mass range. An outflow powered by a distributed feedback also has a positive radial entropy profile, mimicking what may be produced by a "cooling flow".

(ii) The coronal gas is typically in an approximate hydrostatic state. As a result, the density of the corona gas depends strongly on the thermal pressure of the ICM, but only weakly on the ram pressure. Therefore, the surface brightness of X-ray emission is a good measurement of the thermal ICM pressure, which may be used to estimate the line-of-sight location of a spheroid in a cluster. The total X-ray luminosity of a corona decreases with the increase of the feedback specific energy. The thermal pressure tends to increase (or reduce) the luminosity in subsonic (supersonic) cases.

(iii) The semi-confinement of the coronae by the ICM allows a good constraint on the energetics of the stellar feedback. To be consistent with the observed X-ray luminosity and temperature, the specific energy of the feedback should be $\sim 1.5 - 3$ keV, a factor of 2-3 smaller than the value inferred from the commonly accepted semi-empirical Ia SN and mass-loss rates, assuming the mechanical energy of 10^{51} ergs s^{-1} per SN.

(iv) The relatively high pressure of the coronae in the ICM may have important implications for understanding the AGN activity as well as the cool gas properties in spheroids. The density increase caused by the ICM pressure, for example, could enhance the Bondi accretion, which may explain the observed central concentration of AGNs in clusters. The

high pressure can further compress the gas to form molecular clouds and enhance star formation. The combination of the enhanced consumption and the ram-pressure striping can naturally lead to the deprivation of gas and subsequent passive evolution of galaxies in clusters.

6 ACKNOWLEDGEMENTS

We thank S.-K. Tang for his help in the initial setting up of the simulations. The software used in this work was in part developed by the DOE-supported ASC/Alliance Center for Astrophysical Thermonuclear Flashes at the University of Chicago. Simulations were performed at the Pittsburgh Supercomputing Center supported by the NSF. The project is partly supported by NASA through grant NNX10AE85G.

REFERENCES

Acreman D.M., Stevens I.R., Ponman T.J. & Sakelliou I., 2003, MNRAS, 341, 1333
Bekki K. & Couch W.J., 2003, ApJ, 596, 13
Boroson B., Kim D.W. & Fabbiano G., 2010, arXiv:1011.2529v1
David L.P., Jones C., Forman W., Vargas I.M., & Nulsen P., 2006, ApJ, 653, 207
Edgar R.G., 2004, New Astron. Rev., 48, 843
Eke V.R., Navarro J.F. & Steinmetz M., 2001, ApJ, 554, 114
Fabian A.C., & Sanders J.S., 2009, arXiv:0909.2577
Fryxell B., Olson K., Ricker P., Timmes F.X., Zingale M., Lamb D.Q., MacNeice P., Rosner R., Truran J. W., & Tufo H., 2000, ApJS, 131, 273
Hart Q.N., Stocke J.T. & Hallman E.J., 2009, ApJ, 705, 854
Helsdon S.F. & Ponman T.J., 2003, MNRAS, 340, 485
Hernquist L., 1990, ApJ, 356, 359
Jeltema T. E., Binder B., & Mulchaey J. S., 2009, ApJ, 679, 1162
Kim D.-W., Kim E., Fabbiano G., & Trinchieri G., 2008, ApJ, 688, 931
Knapp G.R., Gunn J.E., & Wynn-Williams C.G., 1992, ApJ, 399, 76
Li Z., Wang Q.D., Irwin J.A., & Chaves T., 2006, MNRAS, 371, 147
Li Z., & Wang Q.D., 2007, ApJ, 668, 39
Li Z., Wang Q.D., & Hameed S., 2007, MNRAS, 376, 960
Machacek M., Dosaj A., Forman W., Jones C., Markevitch M., Vikhlinin A., Warmflash A., & Kraft R., 2005, ApJ, 621, 663
Machacek M., Jones C., Forman W.R., & Nulsen P., 2006, ApJ, 644, 155
Magorrian J., Tremaine S., Richstone D., Bender R., Bower G., Dressler A., Faber S.M., Gebhardt K., Green R., Grillmair C., Kormendy J., Lauer T., 1998, AJ, 115, 2285
Mannucci F., Della Valle M., Panagia N., Cappellaro E., Cresci G., Maiolino R., Petrosian A., & Turatto M., 2005, AA, 433, 807
Martini P., Mulchaey J.S. & Kelson D.D., 2007, ApJ, 664, 761
Mathews W.G. & Brighenti F., 2003, ARAA, 41, 191
Mulchaey J.S. & Jeltema T.E., 2010, ApJ, 751, L1
Navarro J.F., Frenk C.S., & White S.D.M., 1997, ApJ, 490, 493
O'Sullivan E., Ponman T.J., & Collins R.S., 2003, MNRAS, 340, 1375
Sato S. & Tawara Y., 1999, ApJ, 514, 765
Stevens I.R., Acreman D.M. & Ponman T.J., 1999, MNRAS, 310, 663
Sun M., Jones C., Forman W., Nulsen P.E.J., Donahue M., & Voit G.M., 2006, ApJ, 637, 81
Sun M., Jones C., Forman W., Vikhlinin A., Donahue M., & Voit M., 2007, ApJ 657, 197
Sutherland R.S. & Dopita M.A., 1993, ApJS, 88, 253
Tang S., & Wang Q.D. 2010, MNRAS, in press
Tang S., Wang Q.D., Lu Y., & Mo H., 2009, MNRAS, 392, 77
Tang S., Wang Q.D., MacLow M., & Joung M.R., 2009, MNRAS, 398, 1468
Temi P., Brighenti F., & Mathews W.G., 2008, ApJ, 672, 244
Toniazzo T. & Schindler S., 2001, MNRAS, 325, 509
Wang Q.D., 2010, PNAS, 107, 7168
Young J.S. & Scoville N.Z., 1991, ARAA, 29, 581